RSC Advances

PAPER

View Article Online
View Journal | View Issue

Cite this: *RSC Adv.*, 2024, **14**, 16459

Study of the response behavior of a CdS–SnO_2 thick film for high selectivity towards propanol gas

Ankit Kumar Vishwakarma, * Ajaya Kumar Sharma and Lallan Yadava*

Received 12th March 2024
Accepted 30th April 2024

DOI: 10.1039/d4ra01888e

rsc.li/rsc-advances

Gas monitoring devices are in demand for a rapidly growing range of applications. Metal oxide-based gas sensors have been extensively used for the detection of toxic pollutant gases, combustible gases, and hydrocarbon vapors. The sensitivity for a low concentration and observed response and the recovery times of the reported gas sensors are not satisfactory, and it needs further detailed studies. In the present work, undoped SnO_2 and cadmium sulfide (CdS)-doped SnO_2 thick films were fabricated using the screen-printing method to study their sensing behavior towards tested organic vapors such as acetone, propanol, and ethanol. The sensing properties of fabricated sensors were investigated for the test gases, *i.e.* acetone, propanol, and ethanol, at an elevated temperature of 473 K. It was observed that the 2 wt% CdS-doped SnO_2 sensor showed a maximum response (78%) and was highly selective (44.6%) to propanol over acetone and ethanol. The results showed that the diminution of the SnO_2 crystallite size with the CdS content leads to an improvement in the response of the SnO_2 sensor for the tested gases. The microstructural properties are also correlated to the sensing behavior. The measurement showed that the CdS–SnO_2 thick film sensor is highly sensitive. At the same time, it is more selective to propanol than the other test gases, ethanol and acetone.

1. Introduction

In recent years, semiconducting oxide thin/thick films have become more attractive due to their properties such as microstructural and optical properties, high stability, and the excellent sensing devices.[1–4] Semiconducting oxides are classified as n-type and p-type. Currently, p-type semiconducting materials are required for excellent application of the sensor. In particular, SnO_2 is usually regarded as an oxygen-deficient n-type semiconducting material.[5] It has many applications such as transparent conductivity, the electrode of the solar cell, gas sensitivity for gas sensor devices, photochemical and photoconductivity devices in LEDs, and gas discharge display.[6–11] In the sensor technology, the 3S rule is applied, *i.e.*, S = sensitivity, S = selectivity, S = stability. There are various dopants used in the SnO_2 thick/thin film sensor (such as Pd, Ni, Cd, PbO, Fe) to enhance its selectivity and sensitivity and improve its response.[12–15] SnO_2 is used in sensors of combustible gases including carbon monoxide detectors. In these sensors, the sensor area is heated to a constant temperature (a few hundred °C), and in the presence of a combustible gas, the electrical resistivity drops.[16] Doping with various compounds has been investigated (*e.g.*, with CuO).[17] Doping with cobalt and manganese gives a material that can be used in high voltage, for example; in addition, tin(IV) oxide can be doped with the oxides of iron or manganese.[18] J. K. Srivastava *et al.*[19] reported on the microstructural proprieties of the PbO-doped SnO_2 sensor for the detection of methanol, propanol, and acetone. They observed that at 3wt% PbO–SnO_2 gives the maximum response for propanol at 350 °C. They also described the optimization of the firing temperature of the doped SnO_2 sensor for methanol and acetone detection.[12] F. H. Saboor *et al.*[13] presented the NO_2 gas sensing for Pd-loaded SnO_2 thick film gas sensors under UV light irradiation at room temperature. Xi-Tao Yin *et al.*[15] studied the selectivity and sensitivity of a Pd-loaded Fe-doped SnO_2 sensor for CO detection in the presence of H_2, and showed that 10 mol% Fe, 0.2 mol% Pd gives the maximum sensitivity and selectivity to CO against H_2. M. Choudry *et al.*[20] reported the effect of temperature on a Pd-doped SnO_2 thick film gas sensor and observed that the firing temperature at 800 °C gives a more selective sensor for the detection of LPG, H_2, and CH_4, and the reported selectivity of LPG with a maximum sensitivity of up to 87%. In a previous paper, Yadava *et al.*[21] reported on the sensing properties of the CdS-doped SnO_2 thick film gas sensor for the detection of methanol, and showed that the 2wt% CdS-doped SnO_2 sensor is a suitable detector for methanol. In the present study, we report the microstructural properties and sensing response of the CdS-doped SnO_2 thick film. The reduction in crystallite size with the addition of the lower CdS content leads to an improvement in the response of the SnO_2 sensor for the target gases, propanol, methanol, and acetone. The microstructural properties are correlated with the sensing

Thin Film Laboratory, Department of Physics, Deen Dayal Upadhyaya Gorakhpur University, Gorakhpur, U. P., India. E-mail: kv.ankit92@gmail.com; nisaly06@rediffmail.com; Tel: +91 9450253084; +91 7309094050

behavior of the undoped and doped SnO_2 sensors. It is observed that the 2 wt% CdS doped SnO_2 sensor showed a maximum response (78%) and was highly selective (44.6%) to propanol over acetone and ethanol.

2. Experimental

2.1. Synthesis and fabrication of the sensor

In the laboratory, we take tin oxide (SnO_2) powder and glass binder (10 wt% of SnO_2), and mix them properly using a ball mill (Zirconia Ball Mill, Retsch) for 3–4 hours.[21] Fine grains are then mixed with an organic binder (diethyl glycol mono butyl) and organic solvent (α-terpinol) in a ball mill for 1–2 h, which results in an undoped SnO_2 paste. For doped pastes of SnO_2, weighed SnO_2 powder with glass binder (10 wt% of SnO_2) and CdS powder (1 wt%, 2 wt%), all of these components are mixed in a ball mill, and the same organic binder and solvent are used to obtain the sensing paste. The prepared paste is screen-printed on an alumina substrate (25 mm × 25 mm) with a finger electrode pattern on the front side and a resistor heater pattern on the backside, as shown in Fig. 1.

2.2. Characterization and sensing setup

XRD analysis was performed on the structural and lattice parameters of the S_1, S_2, and S_3 films. The D8-Advanced apparatus, connected with a source of Cu $K\alpha_1$ radiation with a wavelength of 0.15406 nm, produced the XRD pattern. For the measurement of the response of the fabricated sensors, S_1, S_2, and S_3, a test chamber has been made in which provisions are made for the electrical connection and inlet/outlet for test gases. The connectivity for the voltage supply and resistance measurement is available through insulated gaskets on the base of the chamber. The resistance of the fabricated sensors in the air and gas environments is measured with the help of a Dual DC power supply (LD-3202) and Digital Multimeter (Aplab 107N). The response of the fabricated sensors is measured in ambient air with varying concentrations of acetone, propanol, and ethanol gases (0–5000 ppm) separately at 473 K.

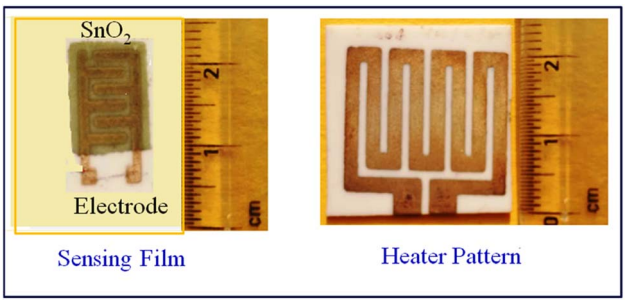

Fig. 1 Finger electrode and heater pattern of the sensor.

3. Result and discussion

3.1. XRD

The experimental XRD pattern of samples S_1, S_2, and S_3 is shown in Fig. 2. The XRD pattern of the fabricated samples has been performed in a wide range of diffraction angles from 0° to 90°. The comparative study of the XRD pattern for the sensors S_1, S_2, and S_3 was performed in diffraction angles from 20° to 55° only. At an angle of 2θ, the peaks of the diffraction pattern correspond to the planes (110), (101), (200), (210), (002), (122), and (301), respectively. The polycrystalline structure of the deposited film is confirmed by these peaks and the correlating planes. If we increase the concentration of CdS in the sensors S_2 and S_3, modification in the XRD pattern is obtained. As we can see from the magnified figure at the plane (200) in Fig. 2(b), the peaks shift toward a higher value of 2θ. As the concentration of CdS increases in the sample, the peak intensities decrease and the peaks are broadening. The crystalline size can be calculated by the well-known formula given by the Debye Scherer relationship.[22,23]

$$D = \frac{\lambda k}{\beta \cos \theta} \quad (1)$$

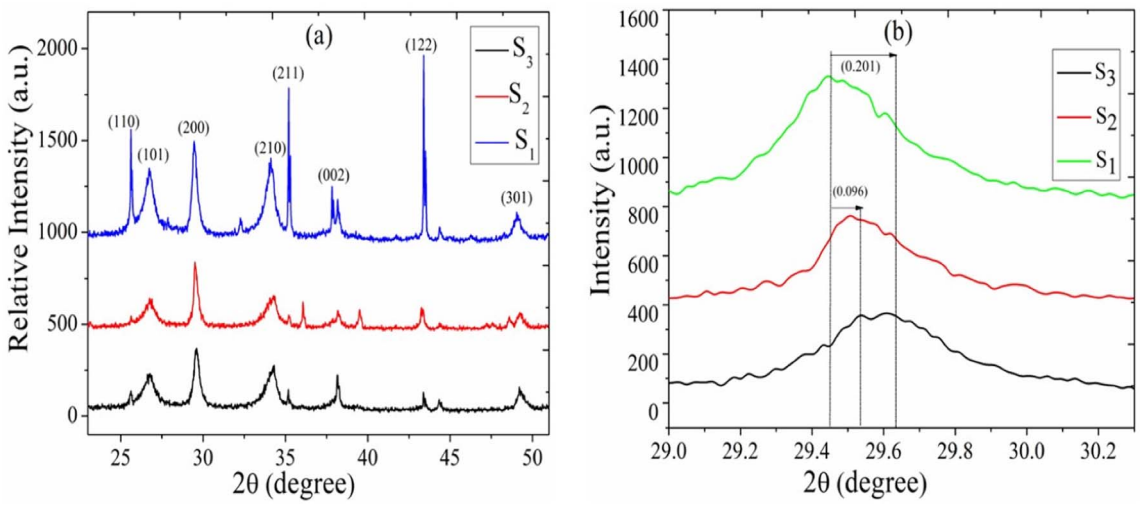

Fig. 2 (a) XRD patterns of sensors S_1, S_2, and S_3 (b) zoomed image of plane 200.

In this case, $k = 0.94$, where λ is the X-ray source's wavelength, β is the full width at half maximum (FWHM), and θ is the diffraction angle. The crystallite sizes of samples S_1, S_2, and S_3 are found at 25.1 nm, 16.1 nm, and 13.9 nm, respectively. This shows that the crystallite size of the SnO_2 films decreases with increasing CdS concentration.

To calculate microstrain, we can use the formula given below:[24]

$$S = \frac{\beta}{4 \tan \theta} \quad (2)$$

The calculated microstrain increases with the increase of the CdS concentration. The crystallite size, rms roughness, and microstrain *versus* the CdS concentration are shown in Fig. 3(a and b), and the calculated value of the microstrain is 0.47 nm, 0.57 nm, and 0.61 nm for S_1, S_2, and S_3. Also, we observed that the crystallite size and roughness decrease with an increase in the CdS contents (Fig. 3(a)).

3.2. Gas sensing response

The sensitivity is defined as the slopes of response *vs.* the gas concentration in ppm. Sensitivity is calculated by the following formula:[25,26]

$$S(\%) = \frac{(R_a - R_g)}{R_a} \times 100 \quad (3)$$

where R_a is the resistance in clean air and R_g is the resistance in the presence of vapors. The response of the fabricated sensors, S_1, S_2, and S_3, are measured with varying concentrations (0–5000 ppm) of the target gases, acetone, ethanol, and propanol, at a fixed operating temperature of 200 °C. The response with the concentration of acetone for sensors S_1, S_2, and S_3 is shown in Fig. 4(a). The response increases with increasing concentration of the acetone vapors. The sensitivity is 36%, 31%, and 25% for the S_3, S_2, and S_1 sensors, respectively. It is evident from Fig. 4(b) that the maximum response for propanol was achieved with the S_3 sensor (78%); it is (1.14) times that of S_2 and (2.79) times that of S_1. The response curve of ethanol is shown in Fig. 4(c). The sensitivity of the fabricated sensor has been reported in Table 1. Fig. 4(d) represents the comparison curve of the S_3 sensor for acetone, ethanol, and propanol. It is observed that sensor S_3 is more sensitive to propanol gas than acetone and ethanol. The sensitivity of propanol for sensor S_3 is 1.34 times that for ethanol and 2.16 times that for acetone. Therefore, propanol has a maximum response compared to the other test gasses. The standard deviation of the response of sensors S_1, S_2, and S_3 for acetone is 5.1, 9.7, and 11.2, respectively. The standard deviation of the response of sensors S_1, S_2, and S_3 for propanol gas is 8.33, 16.97, and 18.87, respectively. The standard deviation of the response of sensors S_1, S_2, and S_3 for ethanol gas is 14.85, 14.01, and 14.46, respectively.

3.3. Selectivity

Selectivity is one of the most important parameters of the sensing properties of the gas sensor. The selectivity of the sensor was calculated using the following formula:[27,28]

$$(\mathrm{Sel})_i = \left[\frac{S_i}{\sum(S_{\mathrm{acetone}} + S_{\mathrm{propanol}} + S_{\mathrm{ethanol}})}\right] \times 100 \quad (4)$$

where S_i is the response of gas for which the relative is to be estimated. The responses were found to be ~45.63%, ~33.91%, and ~20.46% for propanol, ethanol, and acetone, respectively, which is displayed in the histogram (Fig. 5). It is evident from Fig. 4 that propanol is more selective over ethanol and acetone. The standard deviation of the selectivity of S_3 for the gases (acetone, ethanol, and propanol) is 12.59 with a median of 33.91. Recently, N. Barroso *et al.* studied the guest-induced breathing mediated selective alcohol recovery from water by MIL-88A(Fe).[29] They explained how the flexible nature of the crystal structure of MIL-88A(Fe) impacted its adsorptive performance for the recovery of alcohol from water. They found that the results acquired in this work can open new avenues toward the rational design and potential utilization of flexible MOF-based systems, offering enhanced selectivity and sorption performance toward the challenging liquid–liquid separation.

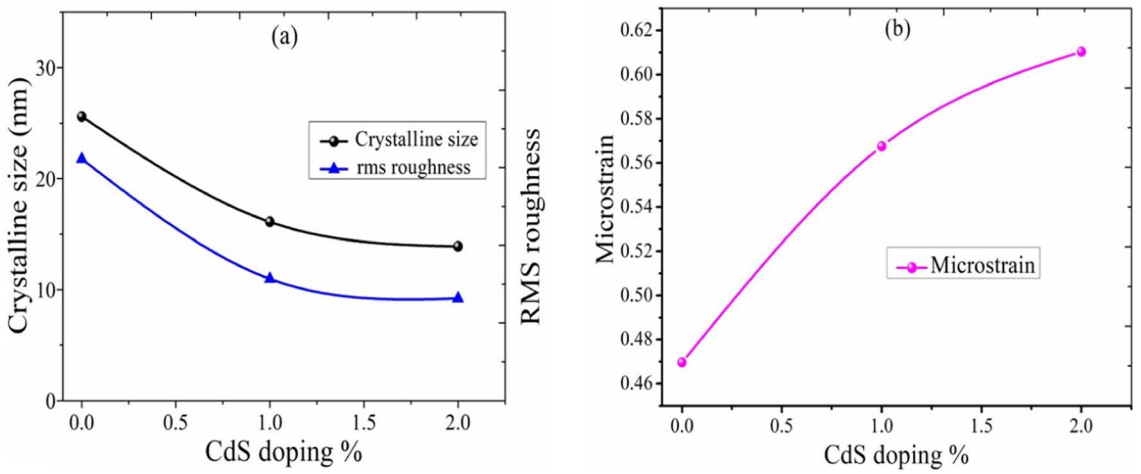

Fig. 3 (a) Variation of the CdS content *vs.* crystallite size, rms roughness. (b) Variation of the CdS content *vs.* microstrain.

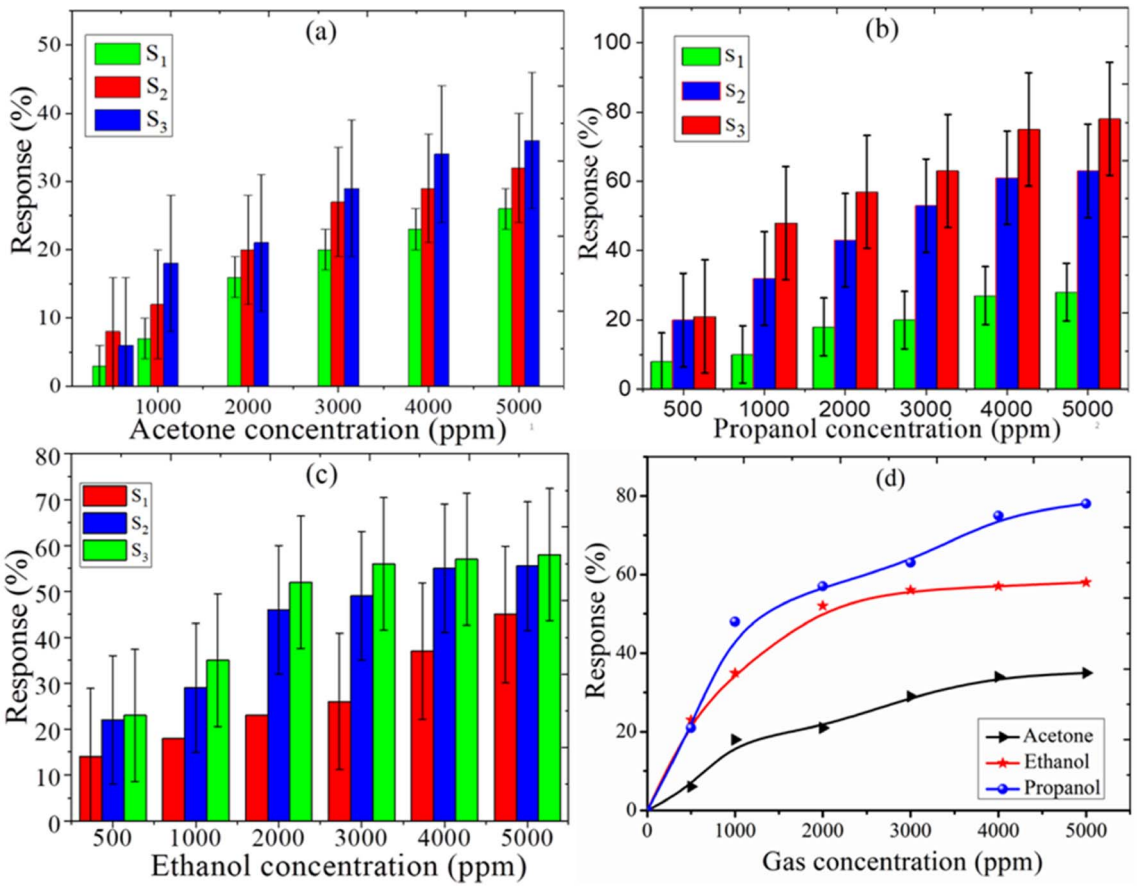

Fig. 4 Sensing response with standard deviation error bars for (a) acetone, (b) propanol, and (c) ethanol gas for sensors S_1, S_2, and S_3. (d) Comparative response with the standard deviation error bars of sensor S_3.

Table 1 Sensing response and selectivity and transient time of the S_3 sensor for propanol, ethanol, and acetone

	Response (%)				Transient time for the S_3 sensor	
Test gas	S_1	S_2	S_3	Selectivity (%)	Response time (s)	Recovery time (s)
Ethanol	45	56	58	33.91	40	70
Propanol	28	65	78	45.63	19	67
Acetone	26	32	36	20.46	45	82

3.4. Transient time

Fig. 4 shows the sensing response *vs.* time of sensors S_3 and S_1 for test gases at 473 K. At time 10 min, 5000 ppm acetone was injected in the test chamber to get the maximum response, and then the chamber was opened to recover the initial state of the sensor. The time corresponds to the time required for the gas response to reach 90% of the final equilibrium value after a test gas is injected, and the recovery time is the time recorded for the gas response to decrease by 90% its maximum value when the gas sensor is exposed in ambient air.[30,31] Fig. 6(b) shows that in the S_3 samples, the fast response and recovery times decrease from 31 s to 19 s and 89 s to 67 s for propanol (5000 ppm at 200 °C), respectively. The transient response and recovery curve to the acetone and ethanol sensors S_1 and S_3 is plotted in Fig. 6(a and c), and its value is listed in Table 1.

3.5. Sensing mechanism

The sensing mechanism of the fabricated sensors (S_1, S_2, S_3) can be realized as the resistance of materials varies with oxygen molecules absorbed at the surface and with the amount of

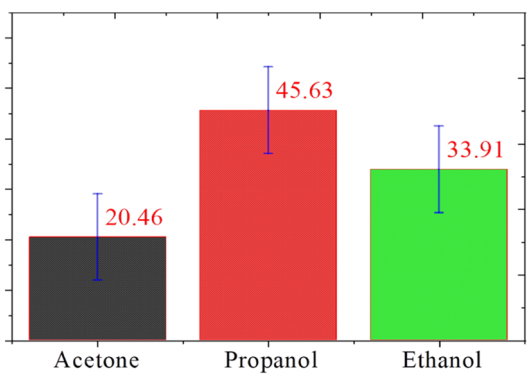

Fig. 5 Selectivity of ethanol, acetone, and propanol gas with standard deviation error bars for sensor S_3.

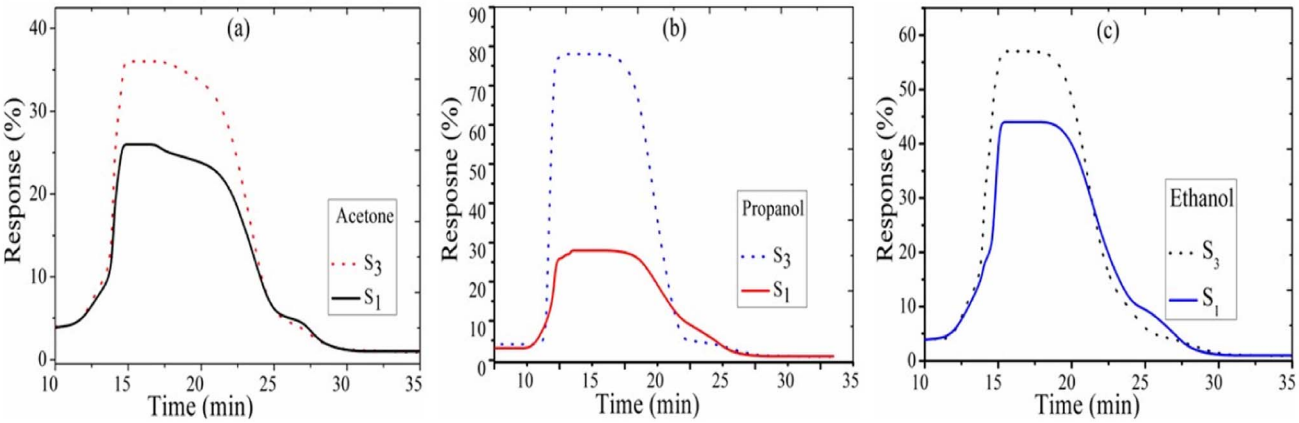

Fig. 6 Transient time for (a) acetone, (b) propanol, and (c) ethanol gas for sensors S_1 and S_3.

reducing gas species. When metal oxide comes in contact with air, the oxygen molecules from the ambient environment are absorbed onto the surface of the metal oxide at the grain boundaries, which trap electrons and build a barrier around each grain.[32] The adsorbed oxygen molecules were subsequently converted to ions after capturing an electron from the conduction band. The adsorbed oxygen exists on the surface in the form of O^-, O_2^-, and O^{2-} species, depending on the temperature.[33] The chemical absorption process can be explained by the following reaction (eqn (5)–(8)):

$$O_{2(gas)} \leftrightarrow O_{2(ads.)} \quad (5)$$

If the operating temperature $T < 150$ °C:

$$O_{2(ads.)} + e^- \leftrightarrow O_{2(ads.)}^- \quad (6)$$

If the operating temperature is 150 °C < T < 400 °C:

$$O_{2(ads.)} + e^- \leftrightarrow 2O_{(ads.)}^- \quad (7)$$

If the operating temperature $T > 400$ °C:

$$O_{2(ads.)} + e^- \leftrightarrow O_{(ads.)}^{2-} \quad (8)$$

When sensor S_3 contacts with the reducing gas, the reducing gas propanol (C_3H_7OH) reacts with the oxygen species to produce carbon dioxide and water, and the resulting electron will return to the conduction band of the semiconductor. The possible surface reactions take place (Fig. 7):

$$C_3H_7OH + 9O^- \rightarrow 3CO_2 + 4H_2O + 9e^- \quad (9)$$

Among the adsorbed oxygen species (O_2-, O^{2-}, and O^-) on the surface, the majorly atomic species (O^- single ionized oxygen) is more reactive, particularly at higher temperatures (150 °C < T < 400 °C). When the CdS–SnO_2 sensor is exposed to the target gases, propanol, ethanol, and acetone, at an elevated temperature of 200 °C, the gas will be adsorbed on the surface of the sensor. These gases will react with the chemically adsorbed oxygen anions, particularly O^-. The electrons are released back to the material of cadmium sulfide, resulting in a decrease in the depletion layer thickness on the surface of the sensor, and also a decrease in the surface band bending. Therefore, the change in the electrical resistance of the sensor is observed with exposure to target gases. Among the target gases, the S_3 sensor showed a larger response and at the same time high selectivity, which may be due to its different molecular structures. Also, it is obvious from eqn (9) that the carrier's concentration increased, which caused the sensor resistance to be reduced. Therefore, this process will increase the carrier concentration on the surface of tin oxide, resulting in a decrease in resistance.[34] For a definite understanding regarding the high selectivity, future work is to be done using an array of sensors and exposure to a mixture of target gases.

We compare our findings to other related work, and a comparison table of the sensing response, operating temperature, and response time for alcoholic and acetone gas is listed in Table 2.

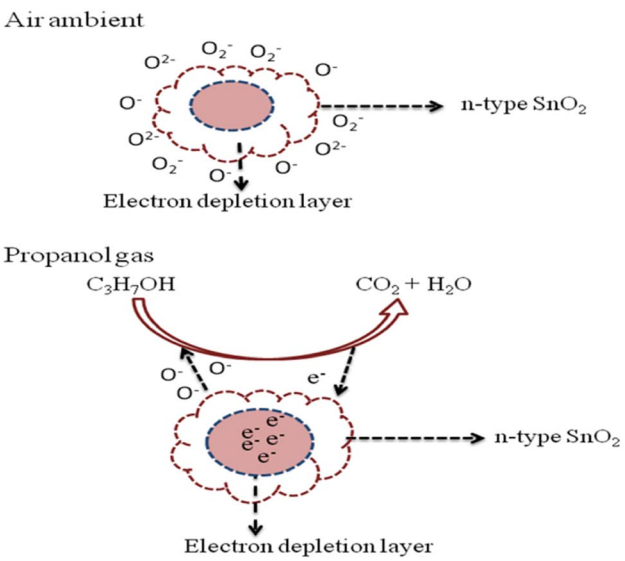

Fig. 7 Reaction process of propanol gas in the SnO_2 thick film.

Table 2 A comparison table of the sensing response, operating temperature, and response time for alcoholic and acetone gas

Sample	Test gas	Operating temperature (°C)	Sensitivity (%)	Response time (s)	References
CdS–TiO_2	Propanol	—	63	62	25
CdS–TiO_2	Acetone	—	71	55	27
Sb_2O_3–SnO_2	Ethanol	250	73.5	—	32
Pd–SnO_2	Ethanol	200	71	41	33
TiO_2	Propanol	—	26	—	34
$LaFeO_3$-based oxide	Propanol	100	258.4	—	35
NiO	Propanol	75	60	—	36
SnO_2	Propanol	150	71	—	37
Pd–SnO_2	Propanol	300	92	—	38
ZnO/TiO_2	Propanol	—	23	10	39
SnO_2 nanorods	Isopropanol	325	11.2	6	40
SnO_2–Pd–Pt–In_2O_3	Methanol	160	320.7	32	41
Ce-doped SnO_2	Acetone	270	50.5	—	42
Cactus-like WO_3–SnO_2	Acetone	360	26	—	43
CdS–SnO_2	Propanol	200	78	19	Present work

4. Conclusion

Three types of sensors, namely S_1 (undoped SnO_2), S_2 (1 wt% CdS–SnO_2), and S_3 (2 wt% CdS–SnO_2), are fabricated. It is found from the XRD pattern that the crystallite size and roughness decrease with dopant CdS (0–2%) and it lies within the anemometric range. The diminution of the SnO_2 crystallite size leads to an improvement in the sensitivity of the fabricated sensors for test gases. Microstructural properties are correlated with the sensitivity of the materials and dopants. The sensing behavior of the sensors S_1, S_2, and S_3 operated at 200 °C for the different target gases (propanol, acetone, and ethanol) under ambient air is reported. The resistance of the sensor decreases with the increasing concentration of gases (0–5000 ppm). It is observed that the 2 wt% CdS-doped SnO_2 sensor showed the greatest response (78%), and is highly selective (44.6%) to propanol over acetone and ethanol with a fast response and recovery time. Thus, we conclude that the CdS doped-SnO_2 thick film sensor is highly sensitive. Furthermore, it is more selective to propanol gas than the other target gases.

Conflicts of interest

The authors declared that they have no competing interests or personal relationships that could have appeared to influence the work reported in this paper.

Acknowledgements

The authors are thankful to the HoD Department of Physics, D. D. U. Gorakhpur University Gorakhpur, for providing experimental facilities.

References

1 F. A. Akgul, C. G. Ali, O. Er and A. H. Farah, *J. Alloys Compd.*, 2013, **579**, 50–56.
2 A. D. Bhagwat, S. S. Sawant and B. G. Ankarmwar, *J. Nano-Electron. Phys.*, 2015, **7**, 04037–04041.
3 S. D. Singh, M. Nand, A. Das and R. S. Ajimsh, *J. Appl. Phys.*, 2016, **119**, 165302–165311.
4 V. Devi, M. Kumar and D. K. Shukla, *Superlattices Microstruct.*, 2015, **83**, 431–438.
5 A. Earnshaw, *Chemistry of the Elements*, Pergamon Press, Oxford, 1984, pp. 447–448, ISBN 0-08-022057-6.
6 J. K. Srivastava, P. Panday and V. N. Mishra, *Sens. Transducers*, 2010, **118**, 122–130.
7 Z. He and I. Zhou, *Mod. Res. Catal.*, 2013, **2**, 13–18.
8 W. Zeng, T. Liu, Z. Wang, S. Tsukimoto, M. Saito and Y. Ikuhara, *Sensors*, 2009, **9**, 9029–9038.
9 J. N. Panchal, S. G. Patel and V. S. Vaishnav, *Sens. Transducers*, 2015, **190**, 35–39.
10 A. Kay and M. Gratzel, *Chem. Mater.*, 2002, **14**(7), 2930–2953.
11 N. Badera, B. Godbole, S. B. Srivastava and P. N. Vishwakarma, *Sol. Energy Mater.*, 2008, **92**, 1646–1651.
12 J. K. Srivastava, P. Panday and V. N. Mishra, *Sens. Transducers*, 2009, **107**, 92–98.
13 F. H. Saboor, T. Ueda, K. Kamada and T. Hyodo, *Sens. Actuators, B*, 2016, **223**, 429–439.
14 M. Choudhary and V. N. Mishra, *J. Mater. Sci.: Mater. Electron.*, 2014, **25**, 1331–1340.
15 Xi-T. Yin and X.-M. Guo, *Sens. Actuators, B*, 2014, **200**, 213–218.
16 W. C-Ming, W. Jin-Feng and S. Wen-Bin, *J. Am. Ceram. Soc.*, 2006, **89**(8), 2502–2508.
17 A. Dibb, M. Cilense, P. R. Bueno, Y. Maniette, J. A. Varela and E. Longo, *Mater. Res.*, 2006, **9**(3), 339–343.
18 A. Punnoose, J. Hays, A. Thurber, M. H. Engelhard, R. K. Kukkadapu, C. Wang, V. Shutthanandan and S. Thevuthasan, *Phys. Rev. B: Condens. Matter Mater. Phys.*, 2005, **72**(8), 054402.
19 J. K. Srivastava, P. Panday, V. N. Mishra and R. Dwivedi, *J. Nat. Gas Chem.*, 2011, **20**, 179–183.
20 M. Choudhary, V. N. Mishra and R. Dwivedi, *Adv. Sci., Eng. Med.*, 2013, **5**, 1–5.

21 L. Yadava, R. Verma and R. Dwivedi, *Sens. Actuators, B*, 2010, **144**, 37–42.
22 A. K. Vishwakarma and L. Yadava, *Vacuum*, 2018, **155**, 214.
23 A. K. Sharma, A. K. Vishwakarma and L. Yadava, *Mater. Lett.: X*, 2023, **17**, 100180.
24 A. K. Vishwakarma, S. S. Majid and L. Yadava, *Vacuum*, 2019, **165**, 239.
25 A. K. Vishwakarma, A. K. Sharma, A. K. Mishra and L. Yadava, *Mater. Lett.: X*, 2023, **17**, 100184.
26 A. K. Vishwakarma, A. K. Sharma and L. Yadava L, *J. Phys.: Conf. Ser.*, 2021, **1921**, 012118.
27 A. K. Vishwakarma, A. K. Sharma A, N. K. Yadav and L. Yadava, *Vacuum*, 2021, **191**, 110363.
28 S. Shao, S. Wang, F. Jiang, H. Wu, T. Wu, Y. Lei, J. Fei and R. Koehn, *R. Soc. Chem. Adv.*, 2016, **6**, 57722–57726.
29 N. Barroso, S. Dutta, O. Castillo, J. Andreo, G. Beobide, A. Luque, S. Perez-Ýañez and S. Wuttke, *J. Mater. Chem. A*, 2023, **11**, 21300.
30 A. K. Vishwakarma, A. K. Mishra, C. K. Dixit and L. Yadava, *Nanomater. Energy*, 2024, **13**, 1–7.
31 A. K. Vishwakarma, A. K. Sharma, A. K. Mishra and L. Yadava, *Mater. Today: Proc.*, 2022, **69**, A18–A21.
32 P. Yadav, S. K. Yadav, A. K. Vishwakarma, D. S. Saini and L. Yadava, *Appl. Phys. A*, 2024, **130**, 119.
33 A. K. Vishwakarma and L. Yadava, *Environ. Sci. Pollut. Res.*, 2021, **28**, 3920.
34 A. K. Vishwakarma and L. Yadava, *IOP Conf. Ser.: Mater. Sci. Eng.*, 2018, **404**, 012020.
35 X. F. Wang, N. Liu, H. Wu, Z. Wan, Y. Meng, Z. Tan and X. Z. Song, *J. Alloys Compd.*, 2023, **954**, 1700217.
36 T. P. Mookoena, K. T. Hillie, H. C. Swart, N. Leshabane, J. Tshilongo and D. E. Motaung, *Mater. Chem. Phys.*, 2020, **253**, 123316.
37 M. Moayedi, H. R. Ansari and Z. Kordrostami, *ECS J. Solid State Sci. Technol.*, 2023, **12**, 057011.
38 R. K. Srivastava, P. Lal, R. Dwivedi and S. K. Srivastava, *Sens. Actuators, B*, 1994, **21**, 213–218.
39 I. Gaidan, D. Brabozon and I. U. Ahad, *Sensors*, 2009, **17**(9), 1995.
40 D. Hu, B. Q. Han, R. Han, S. J. Deng, Y. Wang, Q. Li and Y. D. Wang, *New J. Chem.*, 2014, **38**, 2443–2450.
41 Y. X. Li, D. D Deng, X. X. Xing, N. Chen, L. Xu, X. C. Xiao and Y. D. Wang, *Sens. Actuators, B*, 2016, **237**, 133–141.
42 X. Lian, Y. Li, X. Tong, Y. Zou, X. Liu and D. An, *Appl. Surf. Sci.*, 2017, **407**, 447–455.
43 L. Zhu, W. Zeng and Y. Li, *Mater. Lett.*, 2018, **231**, 5–7.